Elastic properties and electrostructural correlations in ternary scandium-based cubic inverse perovskites: A first-principles study

Maurizio Mattesini*
Departamento de Física de la Tierra, Astronomía y Astrofísica I, Universidad Complutense de Madrid, E-28040 Madrid, Spain

Martin Magnuson, Ferenc Tasnádi, Carina Höglund, Igor A. Abrikosov, and Lars Hultman
Department of Physics, Chemistry and Biology (IFM), Linköping University, SE-58183 Linköping, Sweden
(Received 18 December 2008; revised manuscript received 12 February 2009; published 30 March 2009)

We have performed *ab initio* calculations for the cubic inverse-perovskite Sc_3EN (E=Al,Ga,In) systems to study their electronic band-structures and elastic properties. In this study, we used the accurate augmented plane wave plus local orbital method to find the equilibrium structural parameters and to compute the full elastic tensors. The obtained single-crystal elastic constants were used to quantify the stiffness of the Sc-based ternary nitrides and to appraise their mechanical stability. The site-projected density of states, Fermi surfaces, and the charge-density plots have also been used to analyze the chemical bonding between the Sc_6N cluster and the surrounding metallic lattice of either Al, Ga, or In atoms. Our calculations show that Sc_3GaN has the largest covalent Sc-N bonding-type character with the highest Young, shear, and bulk moduli. Compared with the other two isoelectronic systems, it also behaves as the most brittle material with a relatively large elastic anisotropy.

DOI: 10.1103/PhysRevB.79.125122 PACS number(s): 63.20.dk, 71.20.−b, 74.25.Jb, 74.25.Ld

I. INTRODUCTION

The cubic *inverse* (or anti-) perovskite nitrides (CIPNs) consist of a relatively unexplored branch of perovskite family with captivating electronic properties that can be tuned to give rise either to an insulating or a semiconducting material.[1,2] At present, there exists only a very circumscribed number of ternary early transition-metal CIPNs, which can be summarized as Ti_3AlN,[3] Sc_3InN,[4] and the latest synthesized Sc_3AlN.[5] For the latter, a comprehensive experimental study of the electronic structure and chemical bonding has been recently given in Ref. 6. Nevertheless, a systematic and thorough theoretical investigation of the electronic band structure has not previously been reported for the Sc-based systems. A detailed knowledge of the electrostructural properties in inverse perovskites is the key factor for understanding macroscopic phenomena such as high conductivity and elasticity.

Similarly to other early transition-metal nitrides, the Sc-based CIPNs represent a class of compounds that could have important technological applications as multifunctional hard wide-band-gap semiconductors and also in magnetic recording and sensing. However, only two systems, namely, the Al- and In-containing compounds, were synthesized so far. One possibility of finding new Sc-based CIPNs is to seek for thermodynamically stable isoelectronic systems. Practically, this can be achieved by starting from the existing Sc_3AlN and Sc_3InN systems and substituting one (or more) atomic species with the corresponding isoelectronic analog. For instance, the Al atom can be replaced by another element from the same column of the periodic table, so as to keep the total amount of valence electrons. Among various isoelectronic inverse Sc-based perovskites, the Sc_3AlN, Sc_3GaN, and Sc_3InN phases[7] were theoretically predicted to be dynamically stable through phonon spectra investigations; whereas the Sc_3BN was computed to have imaginary vibrational frequencies.[7]

Thus, in this paper, we focus our attention on the physical properties of the newly predicted Ga-containing CIPN (Ga-CIPN) structure by means of first-principles calculations. Specifically, we address the electronic band-structure nature and the mechanical behavior of the hypothetical Sc_3GaN material. The latter is of particular interest as they determine the mechanical stability of the material and important macroscopic properties such as hardness, lubrification, friction, and machinability. The electronic structure investigation will then provide an overall view of electrostructural information that is needed for tailoring and improving the electronic features of this material. The physical characteristics of the Ga-CIPN system are then examined and compared to the specifics of the other isoelectronic Sc_3EN (E=Al,In) stoichiometries.

The structural model used for Sc_3EN is drawn in Fig. 1 and consists of a metallic face-centered lattice formed by Sc and an E element of the IIIb subgroup of the periodic table with a N atom added in the body-centered position. The atomic arrangement of such a cubic structure is basically that of a common perovskite, where the heavy-metal atom (Sc) have exchanged positions with the nonmetal (N) element. The point group around Sc site corresponds to the tetragonal D_{4h}, while for both E and N the symmetry operations reach up those of the cubic (O_h) point group.

The outline of the paper is as follows. In Sec. II we give a brief review of the computational schemes used. The calculations of the structural and electronic properties are developed in Sec. III. The computation of the single-crystal elastic constants is described in Sec. IV, while conclusions are drawn in Sec. V.

II. COMPUTATIONAL METHODS

A. Total-energy calculations

The electronic structures of Sc_3EN, with E=Al, Ga, and In, were computed within the WIEN2K code[9] employing the

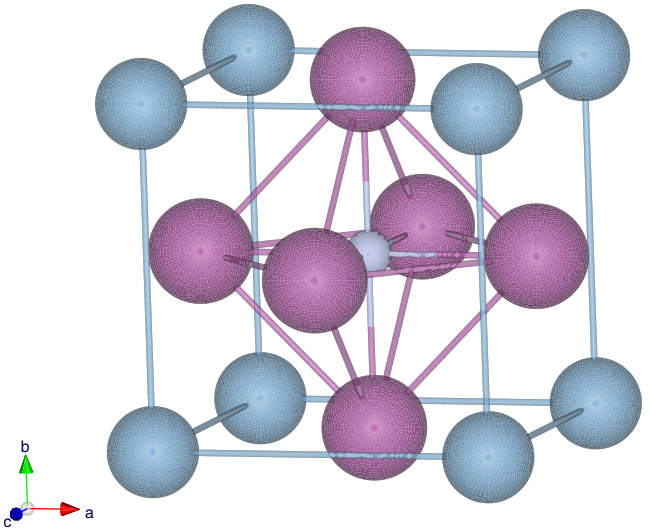

FIG. 1. (Color online) Ball-stick model of the cubic inverse-perovskite Sc_3EN unit cell. Scandium, the IIIb subgroup element (E), and nitrogen are depicted in violet (large spheres), turquoise (medium spheres, at the edges of the cube), and gray (small sphere), respectively. The space group is $Pm\bar{3}m$ (221) with the following Wyckoff positions: Sc $(\frac{1}{2},\frac{1}{2},0)$, E (0,0,0), and N $(\frac{1}{2},\frac{1}{2},\frac{1}{2})$. This figure was created with the VESTA visualization software (Ref. 8).

density-functional[10,11] augmented plane wave plus local orbital (APW+lo) computational scheme.[12] The APW+lo method expands the Kohn-Sham orbitals in atomiclike orbitals inside the muffin-tin (MT) atomic spheres and plane waves in the interstitial region. The Kohn-Sham equations were solved using the recently developed Wu-Cohen generalized gradient approximation (WC-GGA) (Refs. 13 and 14) for the exchange-correlation (xc) potential. It has been shown that this new functional is more accurate for solids than any existing GGA and meta-GGA forms. For a variety of materials, it improves the equilibrium lattice constants and bulk moduli significantly over local-density approximation (LDA) (Ref. 11) and Perdew-Burke-Ernzerhof (PBE) (Ref. 15) and therefore should also perform better for the CIPN systems. For this reason and for testing purposes, we adopted the new WC approximation for the xc potential in studying the Sc_3EN series.

For each system, we first compute the nearest-neighbor distances at their equilibrium geometries and then we determined the optimal set of muffin-tin radii (R_{MT}). The resulting values are listed in Table I. The Sc $(1s^2 2s^2 2p^6)$ states were considered as core states, and they were treated using only the spherical part of the potential. In the same manner, we handled Al $(1s^2 2s^2)$, Ga $(1s^2 2s^2 2p^6 3s^2 3p^6)$, In $(1s^2 2s^2 2p^6 3s^2 3p^6 3d^{10} 4s^2 4p^6)$ states, and the N $(1s^2)$ electrons. For the calculation of the valence part, we considered an expansion of the potential and the charge density into spherical harmonics up to $\ell=6$. The valence wave functions inside the atomic spheres were expanded up to $\ell=10$ partial waves. For Sc, In, and Ga, s, p, and d local orbitals were added to the APW basis set to improve the convergence of the wave function; while, for N and Al, only s and p local orbitals were included. In the interstitial region, a plane-wave expansion with $R_{MT}K_{max}$ equal to eight was used for all the investigated systems, and the potential and the charge density were Fourier expanded up to $G_{max}=8.5$. We carried out convergence tests for the charge-density Fourier expansion using higher G_{max} values and found no significant changes in the calculated electrostructural and mechanical properties. The modified tetrahedron method[16] was applied to integrate inside the Brillouin zone (BZ) and a k-point sampling with a $27\times27\times27$ Monkhorst-Pack[17] mesh in the full BZ (corresponding to 560 irreducible k points) was considered as satisfactory for the cubic Sc_3EN systems. Electronic band-structure calculations were carried out for the CIPN phases by using the relaxed (APW+lo method) unit-cell volumes.

TABLE I. Optimal set of muffin-tin radii used for total-energy calculations. Values are given in a.u. (a_o).

System	R_{MT}(Sc)	R_{MT}(E)	R_{MT}(N)
Sc_3AlN	2.20	2.20	1.90
Sc_3GaN	2.15	2.30	1.91
Sc_3InN	2.20	2.50	1.95
ScN	2.22		1.97

We previously successfully modeled the electronic band structure of the Al-containing CIPN system by using the same kind of theoretical scheme and achieved excellent agreement with experimental data,[6] giving validity and robustness to the present predictions.

B. Fermi surfaces

The Fermi surfaces (FSs) of Sc_3EN, with E=Al, Ga, and In, were also calculated to address the electrical conductivity of the CIPN materials. The calculations for generating FS were carried out by using the QUANTUM-ESPRESSO simulation software package (PWSCF).[18] Since the band structure of these systems is not sensitive to the applied exchange correlation, the calculations were done within the PBE (Ref. 15) approximation. The applied pseudopotentials were taken from the distribution.[19] Convergent Fermi energy (E_F) was achieved with the $(14\times14\times14)$ Monkhorst-Pack sampling of the Brillouin zone.[17] The $(16\times16\times16)$ grid led to convergent and smooth Fermi surfaces calculated from the bands which cross the Fermi energy. The smooth three-dimensional (3D) Fermi-surface plots were generated with the help of the XCRYSDEN molecular structure visualization program[20] applying the tricubic spline interpolation with a degree of 4.

III. STRUCTURAL AND ELECTRONIC PROPERTIES

A. Structure

The calculated equilibrium structural parameters shown in Table II agree fairly well with the reported experimental values for Sc_3AlN, Sc_3InN, and ScN. The theoretical data were computed to be slightly smaller than the experimental ones although all of them are within an error that is less than −0.88%. It is well-known that LDA underestimates the equilibrium lattice constants by 1%–3%, while PBE-GGA often

TABLE II. Structural parameters, single-crystal elastic constants, and averaged polycrystalline properties. The reported numbers within brackets refer to the experimental data. The notation $N_{\text{f.u.}}$ represents the number of f.u. per unit cell.

Property	Sc_3AlN	Sc_3GaN	Sc_3InN	ScN
a (Å)	4.374 (4.40[a])	4.329	4.411 (4.45[b])	4.463 (4.50[c])
V_o (Å^3)	83.695	81.115	85.824	88.914
$N_{\text{f.u.}}$	1	1	1	4
$d_{\text{Sc-N}}$ (Å)	2.187	2.164	2.206	2.232
$d_{\text{Sc-}E}$ (Å)	3.093	3.061	3.119	
$d_{E\text{-N}}$ (Å)	3.788	3.749	3.820	
B (GPa)	114.25	121.19	115.71	219.53
B'	4.088	4.089	4.401	3.783
ρ (g/cm^3)	3.489	4.475	5.102	4.405
C_{11} (GPa)	234.32	268.56	238.57	396.75
C_{12} (GPa)	54.21	47.51	54.28	130.92
C_{44} (GPa)	87.76	92.16	90.76	169.58
G_H (GPa)	88.67	99.11	91.311	153.82
G_H/B	0.776	0.818	0.789	0.701
E (GPa)	211.33 (249[a])	233.65	216.88	374.09 (356[d])
ν	0.192	0.179	0.188	0.216
A	0.980	0.863	0.988	1.185
v_s (km/s)	5.04	4.71	4.23	5.91
v_l (km/s)	8.16	7.52	6.82	9.82
θ_D (K)	647.15	609.66	538.33	871.86

[a]Thin film values from Ref. 5.
[b]Bulk value for the $Sc_3InN_{(0.866\pm0.002)}O_{(0.069\pm0.007)}$ from Ref. 4.
[c]Bulk value from Ref. 21.
[d]Thin-film value from Ref. 22.

overcorrects the local-density approximation by predicting values 1%–2% bigger than experiments. Although WC-GGA is thought to be more accurate than both LDA and GGA, one should bear in mind that experimental lattice constants must be extrapolated down to 0 K to compare with density-functional theory (DFT) values. This is due to the effect of thermal expansion and to the zero-point quantum fluctuations that are not included in the DFT scheme. Both will enlarge the calculated equilibrium lattice constant. This implies that one should not expect a perfect agreement between the experimental lattice parameters and the computed WC-GGA values. Nonetheless, the search for a remarkable match between experimental and calculated lattice constants goes behind the scope of this work.

B. Electronic density of states

The partial density of states (PDOSs) were calculated for the fcc-ScN (rocksalt) and for the CIPN Sc_3EN systems by using their equilibrium geometries. Figures 2–5 show the decomposed density of states (DOS) computed at the WC-GGA level. From Fig. 2 one can see that the partial DOS in rocksalt ScN structure presents a rather strong hybridization between the valence s, p, and d states of Sc and the s and p orbitals of nitrogen, underlining the considerable covalent-

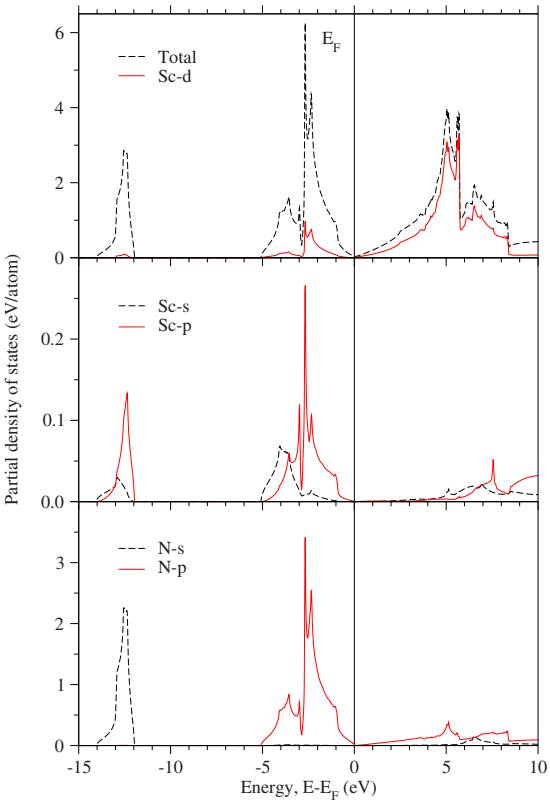

FIG. 2. (Color online) Partial density of states for the rocksalt ScN structure.

like nature of the Sc-N bonding. The electronic ground state of ScN is therefore characterized by atomic species that tend to share part of their valence electrons as to form strong directional bonds. An energy gap of 7 eV has been computed in between the energy positions of the N 2s and N 2p states. The WC-GGA functional also predicts that there is no band gap (E_g) for rocksalt ScN with a PDOS that goes rapidly to zero at E_F. For comparison, we here remind that an experimental band gap of 0.9 ± 0.1 eV was measured for ScN.[23] This indicates that the DFT-WC-GGA scheme is only in part able to reproduce the semimetallic character of the ScN system.

Substitution of either Al, Ga, or In in the Sc_3EN stoichiometry would nominally keep the same electronic charge in the s and p valence bands (VBs). This is somewhat confirmed by the calculated density of states of Al, Ga, and In nitrides, which are characterized by the same DOS features. Apart from the atomiclike (i.e., localized) nature of the Ga and In d states, the calculated PDOSs for the three isoelectronic Sc_3EN systems appear rather delocalized (i.e., wide bands), which usually makes electronic band-structure calculations appropriate for the interpretation of nonresonant emission spectra.[6] For Sc_3AlN (Fig. 3), the group of high-lying electronic states (−7.0 to 0 eV) relates to both metal-metal (Sc-Al) and metal-nonmetal (Sc-N) interactions. Just below the Fermi energy, the Al 3p states hybridize strongly with the electronic states of Sc, while the interaction between Sc and N 2p states has been found at ~2 eV deeper in energy.

For Ga- and In-containing CIPN structures, we found that both $3d^{10}$ and $4d^{10}$ band states are very much localized at

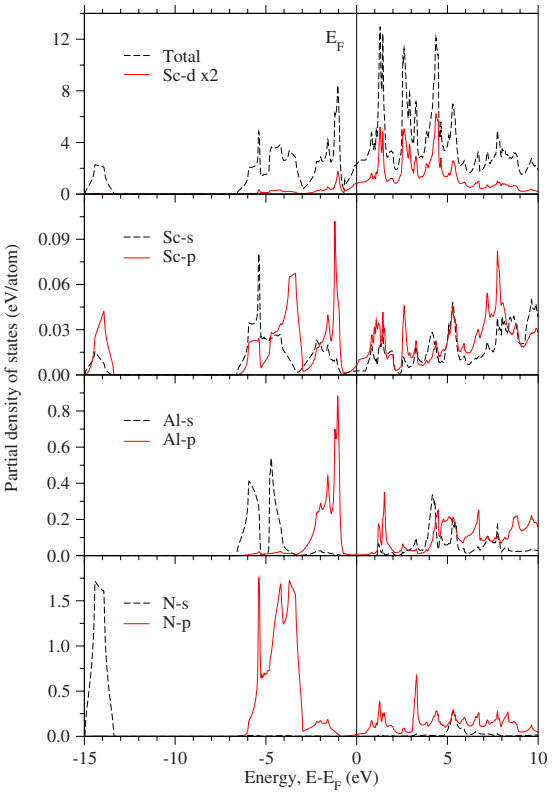

FIG. 3. (Color online) Partial density of states for the Sc_3AlN system.

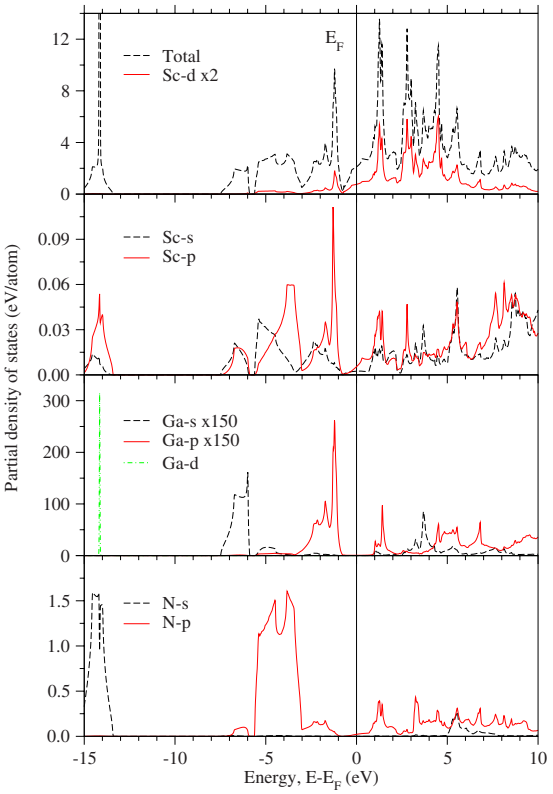

FIG. 4. (Color online) Partial density of states for the Sc_3GaN system.

around −14 eV. Although they are centered at the same energy position of the Sc *s*, *p*, *d*, and N *s* bands, they are not hybridizing very much with them as shown by the different size of band dispersion. The main difference between the PDOS of Sc_3AlN and those of Ga- and In-CIPN systems was found on the bandwidths related to the electronic states located in between 0 and −7.5 eV. Gallium and indium phases are showing a clear energy overlap between the *s* states of the *E* atom and the *p* states of N in an energy range that is comprised between −5 and −7.5 eV. Such kind of electronic states mixing is almost absent in the Al-CIPN model. The calculated electronic bands of Ga- and In-containing structures are therefore 0.84 and 0.68 eV, respectively, wider than the analogous Al system. Generally speaking, the spreading of such electronic bonding states by almost 1 eV can be taken as an indication of an increased covalent character.

At E_F, the density of states of all the CIPN structures are mainly from Sc *d* states with a small admixture of N *p* states. These phases can therefore be classified as metallic materials, thus confirming the latest experimental finding for Sc_3AlN.[5] The bottom of the conduction band (CB) is primarily determined by the unoccupied Sc *d* states (i.e., the three characteristic peaks) that are mixed with both the *E s*, *p* orbitals, and the *p* states of N.

For free electrons, the electrical conductivity would be proportional to the number of states at the Fermi energy $N(E_F)$, which is largely governed by the Sc-*E* metal bonding. Although indications of electron correlations are found in the studied materials,[6] it is useful to compare the trend in the conductivity with the density of states at the E_F. The calculated $N(E_F)$ in units of states eV^{-1} $cell^{-1}$ are 2.31, 2.13, and 2.30 for Sc_3AlN, Sc_3GaN, and Sc_3InN, respectively. Within this simplified picture, the electrical conductivity in Sc_3GaN should be slightly lower than the two other CIPNs.

C. Valence electron-density maps

We hereby investigate possible modifications in the Sc-N bonding topology when inserting a simple-cubic (sc) *E* lattice all around the Sc_6N cluster. Namely, from the analysis of the difference electron-density maps, one can get deeper insight about the covalent nature of the Sc-N bond for the three isoelectronic nitrides.

We first start by studying the charge-density distribution in the simple ScN rocksalt structure. The contour density plot taken along the [001] plane (see Fig. 6) reveals areas with a considerable charge accumulation (at N sites) and dissipation (at Sc sites) as to indicate that charge transfer is not a negligible effect in ScN rocksalt crystal. Most of the electronic charge that has been transferred to the N atoms is taken from regions (see green-blue isolines of in Fig. 6) where the covalent Sc-Sc interactions are taking place.

To disclose the effect of a metallic *E* lattice enveloping the Sc_6N atomic moiety, we further calculated the ground-state valence charge densities of Sc_3EN models and those of the structural analogous Sc_6N systems. The latter was computed by keeping the optimized crystal geometry of the Sc-based ternary nitrides and removing the *E* atom from their cubic unit cells. The obtained contour plots for the resulting density differences are shown in Fig. 7. We found that the

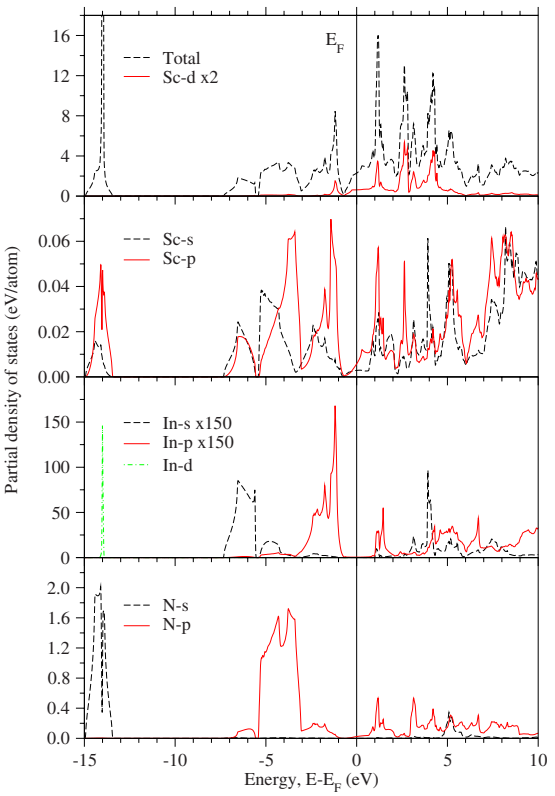

FIG. 5. (Color online) Partial density of states for the Sc_3InN system.

metallic E lattice has the common effect of redistributing a considerable amount of electron density from Sc atoms, thus modifying the bonding nature and strength of the Sc-N

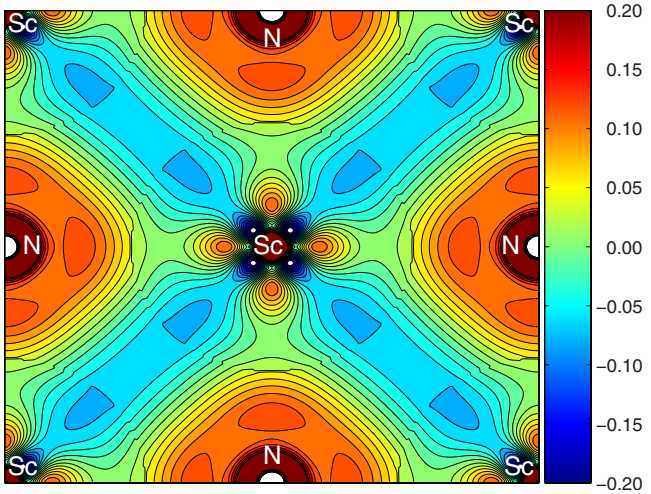

FIG. 6. (Color online) Difference valence electron-density plots [i.e., $\Delta n(r)$, crystalline minus superposed atomic densities] for rock-salt ScN. Contour plot was obtained by subtracting the atomic valence charge densities (in units of $e/\text{Å}^3$) along the [001] plane of the cubic cell. The scale used for coloring is shown at the right-hand side of the plot. Red-yellow (positive) zones denote regions of charge accumulation and green blue (negative) denotes regions of charge depletion. The lower valence-band energy was fixed to −17.70 eV, as to catch the Sc $3d^14s^2$ and N $2s^22p^3$ valence states.

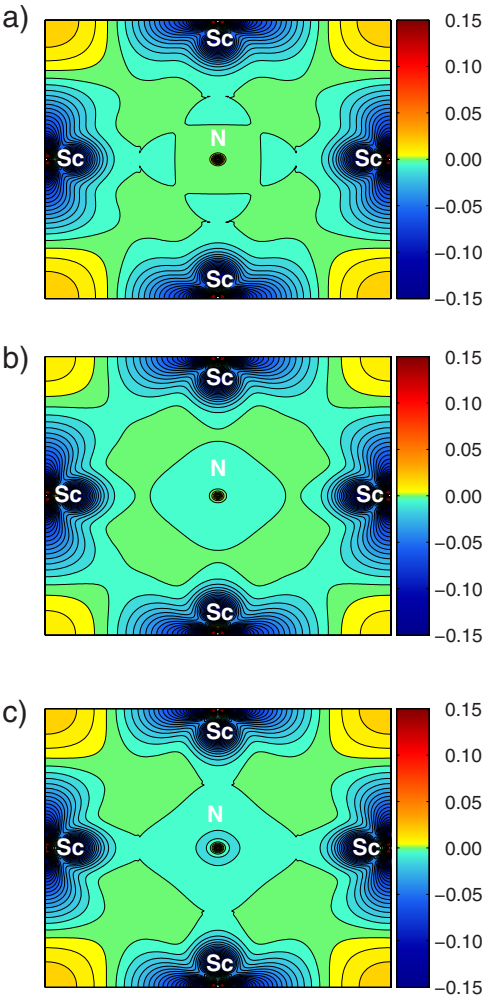

FIG. 7. (Color online) Calculated electron-density difference plots between Sc_3EN and the Sc_6N cluster in the same crystal geometry for (a) Sc_3AlN, (b) Sc_3GaN, and (c) Sc_3InN. These plots were obtained by subtracting the valence charge density in the [200] plane of the cubic inverse-perovskite structure. Positive values implies gain of density and negative values loss of density (in units of $e/\text{Å}^3$).

bonds. Inset (a) of Fig. 7 shows that a sc Al-lattice also removes a small quantity of charge along the directional Sc-N bonds with a consequent enhancement of the ionic bonding character. Note that no charge-density removal has been found at the central N atom.

On the other hand, when looking at Ga CIPN, we observed that Ga tends to take out electron density from the central N atom in a spherical way and to preserve more the original charge density in between the Sc-N bonds. This leads to a more covalentlike Sc-N bonding, which can be attributed to the larger electronegativity of Ga with respect to Al. Therefore, the localized density removal at Sc and N sites weaken the Coulombic-type interactions in the Ga-containing CIPN material. In CIPN locates midway in between Al- and Ga-CIPN systems as it shows both a spherical loss of charge density around the central nitrogen and a density withdrawal along the directional Sc-N interactions. Accordingly, going from Al to Ga (and In) CIPN structures, the Sc-N bonding topology gradually evolves from ioniclike to

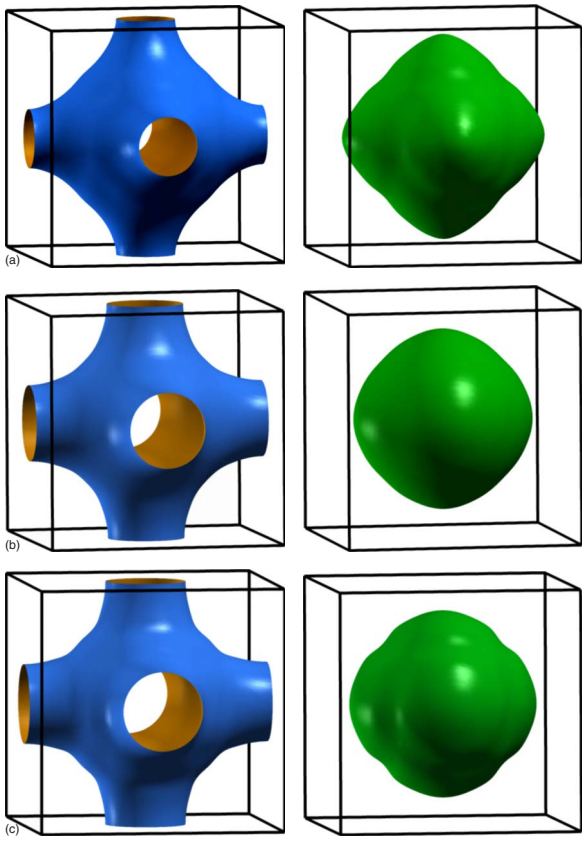

FIG. 8. (Color online) Calculated Fermi surfaces of (a) Sc_3AlN, (b) Sc_3GaN, and (c) Sc_3InN.

covalentlike. As a matter of fact, the Sc_3AlN system is identified by a larger amount of nondirectional interactions, whereas both Ga- and In-CIPN structures are presenting a clear contribution from the bond-bending forces. As we will discuss in Sec. IV, this behavior modifies the elastic properties of the CIPN materials along the Al→Ga→In series.

The Sc-*E* bonding-type has also been identified by a mixed covalent and ionic character, with the shortest bond distance found for the Ga-CIPN and slightly longer ones for both Al and In systems (Table II). This result stems from the fact that Ga is the *E* element that has the largest electronegativity value and a rather small atomic radius. It enhances the electrostatic forces in between *E* and Sc atoms leading to a shorter equilibrium bond length. The decreasing of ionic-like component seen in the difference density maps (not shown here) when going from Al and Ga to In has further been attributed to the increased atomic number (*Z*) and size of the *E* element. The larger *Z* value for In induces a stronger shielding effect at the $5s^25p^1$ valence electrons, thus making them more easily shared with the nearby Sc atom.

D. Fermi surfaces

The calculated Fermi surfaces are shown in Fig. 8. For each Sc_3EN system, one gets two large particle (electron) sheets; both showing close similarity to a free-electron Fermi spheres with closely delineated surfaces. Since mainly the Sc 3*d* electrons are involved around the Fermi energy, the conductivity/metallicity in these systems is determined by these electrons. As one can expect from the DOS shown in Figs. 3–5, the very tiny hybridization between the Sc 3*d* and the other states around the Fermi energy, together with the fact that all the Van Hove singularities are above the Fermi energy, results into a free-electron-like Fermi surfaces.

The equienergy surfaces and so the Fermi surfaces can be discussed within the simple tight-binding picture,[24] where the overlap parameter describes the crystal-field perturbation and also the shape of the band energy dispersion. Since the tight-binding overlap integrals were not directly calculated, we here refer to these integrals as the overlap parameters. The number of states at the Fermi level $N(E_F)$ reflects already a relative tendency for the overlap parameters in the systems under discussion. The increase in the overlap parameter develops a flatlike region in the equienergy surface close to the cubic BZ corner (*R* point), but more importantly it appears as a decrease in the effective mass of the electrons at the Fermi level. In comparison, Sc_3AlN with the relative largest plateau has the strongest crystal-field perturbation described by the largest overlap parameter. Correspondingly, it yields the smallest effective mass for the electrons at the Fermi level. For Sc_3GaN, where the FSs are very similar to smooth spheres, the overlap parameter should be significantly smaller, which indicates that the Sc 3*d* electrons at the Fermi level have the largest effective mass. From this point of view, Sc_3InN is just in between the other two systems, since the distortion of the free-electron Fermi sphere and so the overlap of the Sc 3*d* electrons at the Fermi level is less pronounced. Accordingly, Sc_3AlN shows the most metallic-like conductivity with the smallest effective mass for the electrons at the Fermi level, whereas Sc_3GaN has the less mobile Fermi electrons. For Sc_3InN, the situation is just in between these two cases.

IV. CALCULATION OF THE ELASTIC STIFFNESS TENSOR

The athermal elastic constants $C_{i,j}$ were calculated within the total-energy method, where the unit cell is subjected to a number of finite-size strains along several strain directions. Cubic lattices have three independent elastic constants,[25–27] namely, C_{11}, C_{12}, and C_{44}. These constants obey to the following relations:

$$B = \frac{1}{3}(C_{11} + 2C_{12}), \tag{1}$$

$$C = C_{44}, \tag{2}$$

$$C' = \frac{1}{2}(C_{11} - C_{12}), \tag{3}$$

where *B* is the isotropic bulk modulus, *C* is the resistance to shear deformation across the [100] plane in the [010] direction, and C' is the shear modulus across the [110] plane in the $[1\bar{1}0]$ direction. They can be deduced by straining the lattice vectors according to a isochoric tetragonal deformation, a uniform hydrostatic pressure, and a rhombohedral

shear along the z axis. The tetragonal and rhombohedral distortions were obtained by compressing and expanding the a and c lattice parameters (in a.u. a_o), respectively, by $\pm 2\% \cdot n$ ($n=0-2$). In the case of a uniform hydrostatic distortion, the same degree of unit-cell compression ($-5\% \cdot n$, $n=0-4$) and expansion ($+5\% \cdot n$, $n=0-3$) was applied to all the investigated cubic lattices. The fitting of the energy versus unit-cell volume data set was performed by using the Birch-Murnaghan[28] equation of state (EoS). Since it is essential to keep the R_{MTs} constants and avoid overlapping within a series of calculations, the equation of states was computed by reducing the muffin-tin radii of Table I by 30% and using a $G_{\max}$ value of 13. The tetragonal and rhombohedral strains were carried out within the same criteria by imposing a muffin-tin radius reduction of 5%. The computed nonvanishing single-crystal elastic constants [Eq. (4)] and the EoS parameters are shown in Table II,

$$\mathbf{C}^{\mathrm{cubic}} = \begin{pmatrix} C_{11} & C_{12} & C_{12} & 0 & 0 & 0 \\ C_{12} & C_{11} & C_{12} & 0 & 0 & 0 \\ C_{12} & C_{12} & C_{11} & 0 & 0 & 0 \\ 0 & 0 & 0 & C_{44} & 0 & 0 \\ 0 & 0 & 0 & 0 & C_{44} & 0 \\ 0 & 0 & 0 & 0 & 0 & C_{44} \end{pmatrix}. \quad (4)$$

Not surprisingly, all the calculated C_{ij} values are satisfying Born and Huang's[29] stability criteria for a cubic crystal (i.e., $C_{11} > |C_{12}|$, $C_{11}+2C_{12} > 0$, and $C_{44} > 0$), pointing therefore to mechanically stable systems.

In order to provide a measure of the stiffness of the solid, we compute the so-called Young's modulus (E), which defines the ratio between linear stress and strain. The larger the value of E, the stiffer is the material. The Young's modulus can be calculated by using Hill's[30] shear (G_H) and bulk moduli through the following equation:

$$E = \frac{9BG_H}{3B + G_H}. \quad (5)$$

The value of G_H has been obtained by taking the arithmetic mean of the computed Reuss[31] (G_R) and Voigt[32] (G_V) approximations,

$$G_H = \frac{G_R + G_V}{2}, \quad (6)$$

where

$$G_R = \frac{5(C_{11} - C_{12})C_{44}}{4C_{44} + 3(C_{11} - C_{12})}, \quad (7)$$

and

$$G_V = \frac{C_{11} - C_{12} + 3C_{44}}{5}. \quad (8)$$

The computed Young's moduli are shown in Table II. The theoretical E value for ScN is in a reasonable good agreement with the experimental data, apart from a difference of +18 GPa, which is within the accuracy of our theoretical method. On the contrary, the Sc_3AlN system has a Young's modulus that is ~37 GPa lower than the reported nanoindentation value. Beside the numerical errors that are intrinsic to the DFT-WC-GGA scheme, there will also be a certain degree of uncertainty in determining the experimental Young's modulus for a Sc_3AlN thin film that was grown onto a MgO substrate. The thin-film nature of this sample makes a difficult quantitative comparison with the theoretically predicted elastic modulus. However, as a general tendency, we found that the elastic modulus increases as the covalent character of the system rises. Al-containing CIPN being the softest material and ScN as the hardest one. The fact that Sc_3InN is only a few gigapascals harder than Sc_3AlN can be attributed to the larger size of In atoms that force the system to have a larger lattice constant and hence a longer Sc-N bond length.

The elastic anisotropy of crystals has an important implication in engineering science since it is highly correlated with the possibility to induce microcracks in the materials.[33] The anisotropy factor for cubic crystals,[34] $A=(2C_{44}+C_{12})/C_{11}$, has therefore been evaluated to provide insight on the elastic anisotropy of the present CIPN systems. For a completely isotropic material, that is when $C'=C$, the A factor takes the value of 1, while values smaller or greater than unity measure the degree of elastic anisotropy. It is interesting to note that our calculations give A values close to unity for Sc_3AlN and Sc_3InN: a characteristic of highly isotropic systems. This is further confirmed by the fact that $G \simeq C_{44}$. To the contrary, both ScN and Sc_3GaN are showing a certain amount of elastic anisotropy, which might lead to a higher probability to develop microcracks or structural defects during the growing process. Such a finding is in line with the recently observed phonon softening for the Sc_3GaN phase.[7]

From the computed G_H/B ratios of Table II, one can also estimate the brittle and ductile behaviors of polycrystalline materials by considering B as the resistance to fracture and G_H as the resistance to plastic deformation. Within this *ansatz*, a high (low) G_H/B ratio becomes therefore associated to brittleness (ductility) of materials. Also, the critical number which separates ductile and brittle was fixed at about 0.57.[35] According to the above description, Ga-CIPN behaves as the most brittle model phase, while Al- and In-containing structures have been computed to be slightly more ductile. The more deleterious consequences of brittleness is the sensitivity for thermal shocks, as the material cannot efficiently dissipate thermal stresses via plastic deformations. Thus, a brittle solid can only be subjected to a limited thermal shocks before its strength drops dramatically.

The G_H/B ratios are all within 0.78–0.82 indicating that CIPN structures have bulk modulus exceeding the shear modulus ($B > G_H$). If we further assume that B quantifies the spatially averaged electron density and G_H the nonuniform distribution of the same density, we are now able to estimate the bonding nature directly from the G_H/B ratio. The Ga CIPN shows the largest ratio which corresponds to a larger contribution from the angular stiffness of the covalent directional bonds.

One of the most important parameter that determine the thermal characteristics of materials is the Debye temperature (θ_D). As a rule of thumb, a higher θ_D implies a higher associated thermal conductivity. The knowledge of such a numerical figure is essential for developing and manufacturing electronic devices. In the following, we made use of the simple Debye-Grüneisen model to estimate the magnitude of θ_D for the investigated CIPNs. The Debye temperature can be defined in terms of the mean sound velocity and gives explicit information about lattice vibrations.[36] It can be computed directly from Eq. (9),[37]

$$\theta_D = \frac{h}{k}\left[\frac{3n}{4\pi}\left(\frac{N_A\rho}{M}\right)\right]^{1/3} v_m, \tag{9}$$

where h is the Planck's constant, k is the Boltzmann's constant, N_A is the Avogadro's number, ρ is the density, M is the molecular weight, n is the number of atoms in the unit cell, and v_m is the mean sound velocity given by the following relations:

$$v_l = \sqrt{\left(B + \frac{4}{3}G_H\right)\rho}, \tag{10}$$

$$v_s = \sqrt{\frac{G_H}{\rho}}, \tag{11}$$

and

$$v_m = \left[\frac{1}{3}\left(\frac{2}{v_s^3} + \frac{1}{v_l^3}\right)\right]^{-1/3}. \tag{12}$$

Our first-principles calculations suggest that CIPN phases have a relative high θ_D value as to indicate that they possess a rather stiff lattice and therefore good thermal conductivity. Nonetheless, the obtained Debye temperatures for the three Sc-based nitrides were found to be between 225 and 334 K lower than that of rocksalt ScN. Such a behavior is here addressed to the larger longitudinal and shear sound velocities of the ScN material. The progressive decreasing of mean sound velocities in the Al→Ga→In series further explains the proneness of lowering Debye temperatures along the same sequential order. It is also worth mentioning that our calculated θ_D for ScN (871.86 K) is definitely larger than that of GaN (614.58 K).[38] The computed sound velocities and Debye temperatures are shown in Table II.

The investigation of the elastic properties can be completed by providing the Poisson's ratio (ν), which quantifies the stability of the crystal against shear. This ratio can be defined by using the Hill's limits[30] with the following equation:

$$\nu = \frac{3B - 2G_H}{2(3B + G_H)}. \tag{13}$$

Poisson's ratio can formally take values between −1 and 0.5, which corresponds, respectively, to the lower bound where the material does not change its shape and to the upper bound when the volume remains unchanged. For systems with predominantly central interatomic interactions (i.e., ionic crystals), the value of ν is usually close to 0.25.[39,40] This ratio decreases as noncentral effects become more important. All the calculated Poisson's ratio values are lower than 0.20, which means that CIPNs are affected by a certain amount of noncentral contributions. The lowest ν value has been computed for the Ga-CIPN model phase, as to corroborate the enhanced covalent character of Sc_3GaN with respect to the other isoelectronic cubic inverse-perovskite nitrides.

V. CONCLUDING REMARKS

In summary, this work reports on a study of electrostructural correlation and elastic properties of Sc-based cubic inverse-perovskite nitrides. Our *ab initio* calculations show that Ga and In CIPNs have a more covalent Sc-N bonding type with respect to the Sc_3AlN system. This translates into a larger Young, shear, and bulk moduli. The Sc_3GaN material has been computed to be the most brittle system among the investigated Sc-containing nitrides with the largest elastic anisotropy and the lowest Poisson's ratio. These characteristics might lead to a higher probability of maturing structural defects during the thin-film deposition process. In fact, kinking and kink bands mostly occur in materials with an important degree of anisotropy, while brittleness might render the material difficult to machine, prone to thermal shock, and easily affected by defects during synthesis and processing. This result is in good agreement with early phonon calculations that show a substantial phonon softening for the Sc_3GaN system.

Although all the three investigated Sc-based CIPNs are isoelectronic to each other, we have shown in Sec. III that a precise trend in the covalent Sc-N bonding character can be found when going down the column of the IIIb subgroup elements. Specifically, from the analysis of partial DOSs and valence electron-density maps, we were able to identify a clear variation in the nature of the Sc-N bond when introducing a sc Ga lattice all around the Sc_6N cluster. To address this different bonding topology in the various CIPN systems, we used the following physicochemical scenario. When inserting a metallic lattice of E atoms all around the Sc_6N cluster, one indirectly modifies the nature of the Sc-N bonding. The tabulated[41] Pauling electronegativity values for Al, Ga, and In are all larger than that of Sc (1.36) and lower than N (3.04) and corresponds to 1.61 (Al), 1.81 (Ga), and 1.78 (In), being Ga the atomic species with the largest electronegativity. Hence, when a sc lattice is constituted by Ga atoms, the electron withdrawing effect from E to the Sc atom reaches up its maximum with the general outcome of creating a more covalentlike Sc-N bond. This simple atomic property, together with the relatively large atomic radius of In, allows to explain the trends found in the obtained lattice parameters, bond distances, and covalent/ionic character along with the three isoelectronic Sc-based nitrides.

Finally, from the computed Fermi surfaces, we observed that Sc_3AlN has the most metalliclike conductivity with the smallest effective mass for the electrons at E_F, whereas the Ga-containing system presents the less mobile Fermi electrons.

ACKNOWLEDGMENTS

The authors acknowledge financial support by the Spanish Ministry of Education and Science through the Ramón y Cajal program and the project of the Plan Nacional I+D+i 2008-2011 (Grant No. CGL2008-00891). This work was also supported by the Swedish Research Council (VR) Linnaeus Grant. I.A.A. and F.T. are grateful to Strategic Materials Research Center on Materials Science for Nanoscale Surface Engineering (MS^2E) supported by the Swedish Foundation for Strategic Research (SSF) and to the Göran Gustafsson Foundation for Research in Natural Sciences and Medicine. The computations of this study were carried out in the *Aula SUN Microsystems* of the Universidad Complutense de Madrid.

*Author to whom correspondence should be addressed; mmattesi@fis.ucm.es

[1] M. Y. Chern, D. A. Vennos, and F. J. DiSalvo, J. Solid State Chem. **96**, 415 (1992).
[2] R. Niewa, W. Schnelle, and F. R. Wagner, Z. Anorg. Allg. Chem. **627**, 365 (2001).
[3] J. C. Schuster and J. Bauer, J. Solid State Chem. **53**, 260 (1984).
[4] M. Kirchner, W. Schnelle, F. R. Wagner, and R. Niewa, Solid State Sci. **5**, 1247 (2003).
[5] C. Höglund, J. Birch, M. Beckers, B. Alling, Z. S. Czigány, A. Mücklich, and L. Hultman, Eur. J. Inorg. Chem. **2008** (8), 1193 (2008).
[6] M. Magnuson, M. Mattesini, C. Höglund, I. A. Abrikosov, J. Birch, and L. Hultman, Phys. Rev. B **78**, 235102 (2008).
[7] A. S. Mikhaylushkin, C. Höglund, J. Birch, Z. S. Czigány, L. Hultman, S. I. Simak, B. Alling, F. Tasnadi, and I. A. Abrikosov, Phys. Rev. B (to be published).
[8] K. Momma and F. Izumi, J. Appl. Crystallogr. **41**, 653 (2008).
[9] P. Blaha, K. Schwarz, G. K. H. Madsen, D. Kvasnicka, and J. Luitz, *WIEN2k: An Augmented Plane* Wave+Local *Orbitals Program for Calculating Crystal Properties* (Karlheinz Schwarz/Techn. Universität Wien, Austria, 2001).
[10] P. Hohenberg and W. Kohn, Phys. Rev. **136**, B864 (1964).
[11] W. Kohn and L. J. Sham, Phys. Rev. **140**, A1133 (1965).
[12] E. Sjöstedt, L. Nordström, and D. J. Singh, Solid State Commun. **114**, 15 (2000).
[13] Z. Wu and R. E. Cohen, Phys. Rev. B **73**, 235116 (2006).
[14] F. Tran, R. Laskowski, P. Blaha, and K. Schwarz, Phys. Rev. B **75**, 115131 (2007).
[15] J. P. Perdew, K. Burke, and M. Ernzerhof, Phys. Rev. Lett. **77**, 3865 (1996).
[16] P. E. Blöchl, O. Jepsen, and O. K. Andersen, Phys. Rev. B **49**, 16223 (1994).
[17] H. J. Monkhorst and J. D. Pack, Phys. Rev. B **13**, 5188 (1976).
[18] QUANTUM-ESPRESSO is a community project for high-quality quantum-simulation software, based on density-functional theory, and coordinated by Paolo Giannozzi; see http://www.quantum-espresso.org and http://www.pwscf.org.
[19] http://www.quantum-espresso.org
[20] A. Kokalj, Comput. Mater. Sci. **28**, 155 (2003).
[21] W. Lengauer, J. Solid State Chem. **76**, 412 (1988).
[22] D. Gall, I. Petrov, N. Hellgren, L. Hultman, J.-E. Sundgren, and J. E. Greene, J. Appl. Phys. **84**, 6034 (1998).
[23] H. A. Al-Brithen, A. R. Smith, and D. Gall, Phys. Rev. B **70**, 045303 (2004).
[24] C. Kittel, *Introduction to Solid State Physics* (Wiley, New York, 1996).
[25] J. F. Nye, *Physical Properties of Crystals: Their Representation by Tensors and Matrices* (Oxford University Press, Oxford, 1985).
[26] M. Mattesini, R. Ahuja, and B. Johansson, Phys. Rev. B **68**, 184108 (2003).
[27] M. Mattesini, J. M. Soler, and F. Ynduráin, Phys. Rev. B **73**, 094111 (2006).
[28] F. Birch, Phys. Rev. **71**, 809 (1947).
[29] M. Born and K. Huang, *Dynamical Theory of Crystal Lattices* (Clarendon, Oxford, 1956).
[30] R. Hill, Proc. Phys. Soc. London **65**, 396 (1952).
[31] A. Reuss, Z. Angew. Math. Mech. **9**, 49 (1929).
[32] W. Voigt, *Lehrburch der Kristallphysik* (Teubner, Leipzig, 1928).
[33] V. Tvergaard and J. W. Hutchinson, J. Am. Ceram. Soc. **71**, 157 (1988).
[34] B. B. Karki, L. Stixrude, S. J. Clark, M. C. Warren, G. J. Ackland, and J. Crain, Am. Mineral. **82**, 51 (1997).
[35] S. F. Pugh, Philos. Mag. **45**, 823 (1954).
[36] A. M. Ibrahim, Nucl. Instrum. Methods Phys. Res. B **34**, 135 (1988).
[37] O. L. Anderson, J. Phys. Chem. Solids **24**, 909 (1963).
[38] L. Y. Lu, X. R. Chen, Y. Cheng, and J. Z. Zhao, Solid State Commun. **136**, 152 (2005).
[39] M. H. Ledbetter, *Materials at Low Temperatures*, edited R. P. Reed and A. F. Clark (American Society for Metals, OH, 1983).
[40] V. V. Brazhkin, A. G. Lyapin, and R. J. Hemley, Philos. Mag. A **82**, 231 (1992).
[41] A. M. James and M. P. Lord, *Macmillan's Chemical and Physical Data* (Macmillan, London, 1992).